Emergent dynamics in excitable flow systems

Miguel Ruiz-García and Eleni Katifori
Department of Physics and Astronomy, University of Pennsylvania, Philadelphia, Pennsylvania 19104, USA

(Received 22 March 2020; accepted 26 April 2021; published 3 June 2021)

Flow networks can describe many natural and artificial systems. We present a model for a flow system that allows for volume accumulation, includes conduits with a nonlinear relation between current and pressure difference, and can be applied to networks of arbitrary topology. The model displays complex dynamics, including self-sustained oscillations in the absence of any dynamics in the inputs and outputs. In this work we analytically show the origin of self-sustained oscillations for the one-dimensional case. We numerically study the behavior of systems of arbitrary topology under different conditions: we discuss their excitability, the effect of different boundary conditions, and wave propagation when the network has regions of conduits with linear conductance.

DOI: 10.1103/PhysRevE.103.062301

I. INTRODUCTION

Flow networks appear in a multitude of natural and artificial systems that require efficient distribution of nutrients, goods, or any other quantity of interest through the system. They are composed of a set of connections (e.g., resistors in the context of an electrical current network) that carry the flow between nodes. They also possess an external input (akin to an electric battery or a fluid pump) that provides the necessary energy for the flow to overcome energy losses due to dissipation. A widely studied example of a natural flow network is the vascular system of plants and animals, whereas an artificial one is the power grid or water distribution systems.

Since the seminal work of Kirchhoff in 1847 [1], much success has been achieved modeling flow systems as networks of linear resistors (see, e.g., [2]). These models present interesting physics; however, their linear nature, and absence of elements such as capacitors and inductors, assumes that a change on the boundary conditions (the net currents or pressures specified at a predetermined set of nodes, termed the *contacts*) is instantaneously transmitted to the entire system. Thus, when the boundary condition (e.g., the voltage drop in the battery) is specified, there is a unique solution (up to a gauge) for the pressures throughout the system, and the dynamics of the whole system can be straightforwardly inferred from the dynamics imposed at the boundary nodes.

In this work we revisit the physics of resistor networks by relaxing the linearity condition. We consider a system of nonlinear resistors, with a nonlinear relation between the current flowing through a link (i, j) and the pressure difference between the two nodes i and j. We demonstrate that such a system can exhibit complex dynamics even in the absence of a time-dependent drive. In our model, in contrast to simple linear resistor networks, the spatiotemporal variations of the current require that we consider transient internal storage of fluid. In the vascular system, for example, this is something that is accomplished by the dilation of the vessels. In our model we introduce this property by allowing, and accounting for, accumulation of volume at the network nodes. This enables the propagation of pressure and volume perturbations along the system.

The one-dimensional (1D) limit of our model is related to previous models used to study semiconductor superlattices [3,4]. These models can present complex dynamics such as self-sustained oscillations [3] or chaotic behavior [5,6]. Also, its continuum limit has been used to study the Gunn effect in semiconductors [7]. Our model uses equations consistent with the scaling laws of fluidic systems rather than with semiconductor electronics. Unlike the previous work, it can be used on networks of arbitrary topology.

We focus our attention on the parameter range that displays oscillatory behavior under constant boundary conditions. Moreover, the model presented in this work displays the basic properties characterizing excitable dynamical systems. In particular, for some parameter range, the system presents a stable point; and when perturbed away from it, it makes a large excursion in phase space before returning to the stable point. This is the signature behavior of excitable models [4,8]; we show an example of this behavior in Sec. IV B 2 and in Fig. 7. Other models of excitable networks have been previously studied, but these models usually include explicitly excitable elements at the nodes of the network. These elements can belong to different classes: they can be discrete variables that can be in a resting, excited, or refractory state and that can excite their neighbors (see [9]); or they can be neuron-like continuous variables whose dynamics are coupled to their neighbors' dynamics (see, e.g., [10]). In our case the nodes are not intrinsically excitable but just store volume. Excitability emerges as a global effect that stems from the combination of (1) the coupling between the node capacity and the pressure field and (2) the nonlinear conductance. This combination gives rise to the complex dynamics shown, at least in part, in this work.

The paper is structured in the following way. We first describe the mathematical model in Sec. II. In Sec. III we present the basic rationale for the emergence of spontaneous

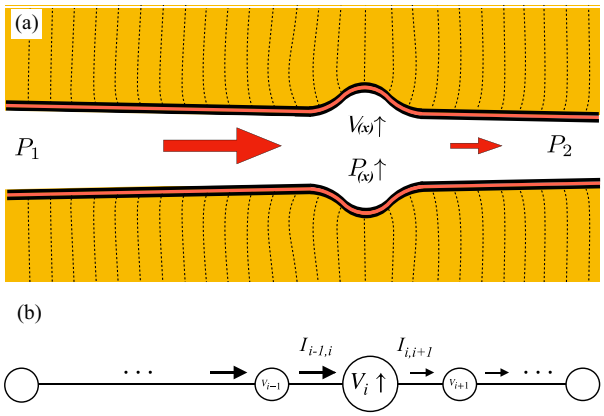

FIG. 1. Sketch representing a section of a flexible tube (vessel) immersed in an elastic surrounding medium (a) and its network counterpart (b). (a) The pressure is set at the entrance and exit of the tube, driving flow from left to right (red arrows). The pressure in the tube decays from P_1 to P_2. Due to a nonlinearity in the flow-pressure relation, present in biological systems (see Appendix B) or in microfluidic networks [11–13], the flow can diminish in one region of the tube (smaller arrow). This causes a volume accumulation in the preceding region at x that subsequently makes the pressure locally increase in the same region. This accumulation deforms the surrounding medium modifying the pressure far from the accumulation region as well (see Appendix A). Note that, depending on the relation of the flow to the pressure gradient, this accumulation can decrease and vanish, returning the system to the original configuration, or it can grow to a new stable solution, such as a traveling wave. The dashed lines display the internal displacements in the surrounding medium due to the volume accumulation in the vessel. (b) The 1D discrete network modeling the continuous system in (a) conserves the basic ingredients that explain the emergence of the complex dynamical behavior. The volume V_i is stored in the nodes $\{i\}$, and it can vary with time, and the edges carry the currents $I_{i-1,i}$ between them.

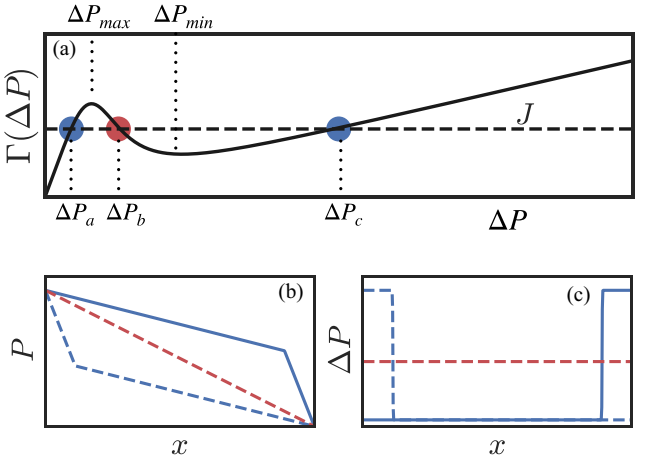

FIG. 2. Plots depicting the construction of piecewise profiles in the 1D model. (a) Generic plot of $\Gamma(\Delta P)$ versus ΔP (continuous line). The three highlighted points correspond to pressure differences ΔP such that $\Gamma(\Delta P_a) = \Gamma(\Delta P_b) = \Gamma(\Delta P_c) = J$. The red point ($\Delta P_b$) corresponds to an unstable configuration, whereas the two blue points (ΔP_a and ΔP_c) are locally stable. Panels (b) and (c) show two piecewise profiles in blue with a low-pressure drop region (ΔP_a) and a high-pressure drop region (ΔP_c). Panels (b) and (c) also depict an unstable configuration with $\Delta P_i = \Delta P_b$, in dashed red lines. (b) P versus x (position on the 1D network). The region of the curve with the shallow slope corresponds to ΔP_a and the steeper slope to ΔP_c. (c) ΔP versus x. Note that in the 1D case we use $\Delta P = P_i - P_{i+1}$, making ΔP positive for these profiles. The solid line in (b) and (c) corresponds to the case $\Delta P = \Delta P_a$ followed by $\Delta P = \Delta P_c$, and the dashed line to $\Delta P = \Delta P_c$ followed by $\Delta P = \Delta P_a$.

dynamics with an analytic study of the 1D version of the model. Section IV shows how to numerically solve the model (Sec. IV A) and different examples of interesting phenomenology (Sec. IV B). The discussion of our results is contained in Sec. V.

II. MODEL

The network model is composed of a set of nodes and connections (edges) between them [see Fig. 1(b)]. In contrast to the usual network of linear resistors, we allow for temporal accumulation and depletion of volume in the system. In a system of flexible tubes, the extra volume accumulated by a mismatch between the incoming and outgoing currents in a region of the system produces a temporary expansion of the tubes within this region, increasing their internal volume and compressing the surrounding medium; see Fig. 1 for a sketch showing this effect in a single tube. For simplicity, we account for these volume changes on the nodes of our network. Also, instead of a linear, Ohmic relationship between the pressure drop at the nodes and the current going through the edge that connects them, we consider the connections between the nodes as nonlinear resistors with a region of negative slope (e.g., see Fig. 2).

We define V_i and P_i as the volume and pressure, respectively, at node i of the network. We assume the following expression for the current I_{ij} that goes from node i to node j, through the edge that connects both nodes:

$$I_{ij} = \begin{cases} V_i^2 \Gamma(\Delta P_{ij}), & \text{if} \quad P_i > P_j \\ V_j^2 \Gamma(\Delta P_{ij}), & \text{if} \quad P_j > P_i \end{cases}, \tag{1}$$

where the pressure drop is defined as $\Delta P_{ij} = P_i - P_j$ and $\Gamma(\Delta P)$ is a general function of the pressure drop. For the sake of simplicity, unless otherwise noted, we consider only two kinds of vessels. The first is nonlinear on the pressure drop with one local maximum and one local minimum:

$$\Gamma_{\mathrm{NL}}(\Delta P) = \gamma \frac{\Delta P_o^4 + \epsilon \Delta P^4}{\Delta P_o^4 + \Delta P^4} \Delta P, \tag{2}$$

where ΔP_o is a constant with units of pressure; see Fig. 2. This phenomenological relation may play an important role in biological systems; see Appendix B. Moreover, this type of nonmonotonic relation also can be engineered in microfluidics devices; see, for example, [11,12]. In this work we will also use a linear relation on the pressure drop,

$$\Gamma_{\mathrm{L}}(\Delta P) = h \Delta P. \tag{3}$$

The parameter ϵ is a nondimensional constant and γ and h are constants with dimensions $([V][P][t])^{-1}$, where $[V]$, $[P]$

and $[t]$ are the dimensions for volume, pressure, and time, respectively. From Eqs. (1)–(3) it follows that I_{ij} is positive if $P_i > P_j$ and the current travels from i to j, whereas it is negative if $P_i < P_j$ and the current travels from j to i.

Note that we include a quadratic volume term in the expression for I_{ij} and that $\Gamma_{\rm NL}$ is linear for low-pressure drops, ensuring that we recover the scaling of Poiseuille flow at low pressures. In particular, considering the node volume V_i in the network as a proxy for the volume stored in the region surrounding node i in the real system, we have $V_i \propto R^2$. At sufficiently low ΔP_{ij}, $\Gamma(\Delta P_{ij})$ is linear in the pressure drop and (1) takes the form $I \propto R^4 \Delta P$. Assuming that the length of the vessel (l) and the viscosity of the fluid (μ) do not change, this scales as Poiseuille flow ($I = \pi R^4 \Delta P/8\mu l$). Of course, depending on the specific characteristics of our system, this may be a strong approximation. Nevertheless, a wide range of exponents in the volume factor in Eq. (1) produce self-sustained oscillations; see the Supplemental Material [14]. We also include a relation that couples volume and pressure,

$$V_i - V_R = \alpha_d \sum_k L_{ik} P_k, \tag{4}$$

where V_R is a rest volume and L_{ij} stands for the graph Laplacian. L_{ij} is equal to the degree of i if $i = j$ and -1 if $i \neq j$ but i and j are connected by a link, $L_{ij} = 0$ otherwise. This relationship, connecting pressure and volume, is a phenomenological expression consistent with the physics of flow through an elastic medium (see Appendix A), and it is independent of the currents. When there is an accumulation of volume at one node, expression (4) will result in a pressure distribution in the network that produces currents that will promote the dispersion of the accumulation. When the volume decreases in one node with respect to its neighbors, the pressure field will promote currents that will increase the volume at that node.

Finally, conservation of volume is imposed through

$$\frac{dV_i}{dt} = \sum_k -I_{ik}, \tag{5}$$

where an increment of the volume at one node causes the drop of volume at neighboring nodes.

Without loss of generality we can make the equations dimensionless using $\tilde{V} \equiv \frac{V}{V_R}$, $\tilde{P} \equiv \frac{P}{\Delta P_o}$, and $\tilde{I} \equiv \frac{I}{2\gamma V_R^2 \Delta P_o}$, which sets the dimensionless time to be $\tilde{t} \equiv 2V_R \gamma \Delta P_o t$. With these substitutions, Eqs. (1) to (5) become

$$\tilde{I}_{ij} = \begin{cases} \frac{1}{2}\tilde{V}_i^{\,2}\tilde{\Gamma}(\Delta\tilde{P}_{ij}), & \text{if} \quad \tilde{P}_i > \tilde{P}_j \\ \frac{1}{2}\tilde{V}_j^{\,2}\tilde{\Gamma}(\Delta\tilde{P}_{ij}), & \text{if} \quad \tilde{P}_j > \tilde{P}_i \end{cases}, \tag{6}$$

$$\tilde{\Gamma}_{\rm NL}(\Delta\tilde{P}) = \frac{1 + \epsilon\Delta\tilde{P}^4}{1 + \Delta\tilde{P}^4}\Delta\tilde{P}, \tag{7}$$

$$\tilde{\Gamma}_{\rm L}(\Delta\tilde{P}) = \tilde{h}\Delta\tilde{P}, \tag{8}$$

$$\tilde{V}_i - 1 = \frac{\alpha_d \Delta P_o}{V_R} \sum_k L_{ik}\tilde{P}_k, \tag{9}$$

$$\frac{d\tilde{V}_i}{d\tilde{t}} = -\sum_k \tilde{I}_{ik}, \tag{10}$$

We will also define $\alpha \equiv \frac{\alpha_d \Delta P_o}{V_R}$ so that (9) takes the form

$$\tilde{V}_i - 1 = \alpha \sum_k L_{ik}\tilde{P}_k. \tag{11}$$

In the rest of this work we will drop the tildes for the sake of clarity. Further considerations on alternative expressions for $\Gamma(\Delta P)$ or the possible variations of Eq. (4) may increase the complex dynamical behavior of the model.

III. ANALYTICAL RESULTS: STABILITY AND WAVE PROPAGATION IN ONE DIMENSION

In this section we use the 1D version of our model to explain some of the dynamics exhibited by this system. Here, to simplify the formulas we redefine the pressure difference between two nodes as $\Delta P_i = P_i - P_{i+1}$, and we adopt this sign convention for the rest of this section. Some of the arguments presented here are inspired by the analytical work on semiconductor superlattices. Useful review references of that work can be found in [3,4].

A. Stability of homogeneous stationary profiles

If all the edges (nonlinear resistors) are equivalent, and there is a constant pressure drop at every edge, then $\Delta P_i = \Delta P^*$ and $V_i = 1$. This results in a constant current across the system, a stationary point of the dynamics. For simplicity let us consider here a generic expression for the current $I(\Delta P_i)$ from node i to $i+1$ that depends only on the pressure difference between the two nodes. We also use the coupling between pressure and volume [Eq. (11)], which in the 1D network takes the form

$$V_i - 1 = \alpha(\Delta P_i - \Delta P_{i-1}). \tag{12}$$

Consider now a small perturbation around the stationary state,

$$\Delta P_i = \Delta P^* + \epsilon \Delta p_i, \text{ and } V_i = 1 + \epsilon v_i. \tag{13}$$

Substituting these expressions into Eq. (12) we get

$$v_i = \alpha(\Delta p_i - \Delta p_{i-1}). \tag{14}$$

The conservation of volume in the system is given by

$$\frac{dV_i}{dt} = I(\Delta P_{i-1}) - I(\Delta P_i). \tag{15}$$

Linearizing I around ΔP^* and using (13) and (14) we get

$$\frac{dv_i}{dt} = -\frac{I'(\Delta P^*)}{\alpha} v_i. \tag{16}$$

Now it is clear that a negative slope of $I(\Delta P)$ at ΔP^* will result in an exponential increase of the small perturbations of the accumulated volume (v_i). This is the basic mechanism that renders some of the "trivial" stationary solutions of the model unstable when the current versus pressure drop presents a region of negative slope.

B. Piecewise linear profiles

We now explore when piecewise constant pressure drop profiles are stationary solutions of the dynamics. We consider again a system of N edges arranged on a line. A stationary solution requires the current from one node to the next one

to be constant throughout the whole system. As we have seen in the previous section, if the boundary conditions are the constant external pressures $P_0 = \Pi = N\Delta P_b$ and $P_N = 0$, such that ΔP_b lies on the negative-slope region of $\Gamma(\Delta P)$, the solution $\Delta P_i = \Delta P_b, \forall i \in (0, N)$ is unstable [red dot in Fig. 2(a)]. However, if $\Gamma(\Delta P)$ presents a local maximum followed by a local minimum, as in Fig. 2(a), we can build a different pressure profile containing two regions of constant pressure drop ΔP_a and ΔP_c [blue points in Fig. 2(a)]. These piecewise pressure profiles are presented in Figs. 2(b) and 2(c) as continuous and dashed blue lines. To study if these profiles are stationary solutions of our model, let us assume first that the transition between the regions of low- (ΔP_a) and high- (ΔP_c) pressure drop happens at a single point. This point is situated at k:

$$k = \frac{\Pi - N\Delta P_c}{\Delta P_a - \Delta P_c}, \tag{17}$$

for the continuous line in Figs. 2(b) and 2(c), and at $N - k$ for the blue dashed line. Within the regions with constant pressure drop (ΔP_a and ΔP_c), the volume is 1 and the current is equal to J [see Fig. 2(a)]. However, exactly at the node where the slope of the pressure field changes from ΔP_a to ΔP_c, the volume is different from 1 [due to Eq. (12)]. According to Eq. (6), $I_{k,k+1} \neq J$ while $I_{k-1,k} = J$, and as result $\frac{dV_k}{dt} \neq 0$, showing that this configuration is not a stationary solution of the dynamics.

We will now examine a configuration where the transition between the regions with pressure drop ΔP_a and ΔP_c spans multiple nodes. Like in the previously examined case, we know that the volume at the node situated in the right extreme of the transition region should be 1, to avoid a mismatch in the currents. This can be achieved only exactly in the continuous limit, but let us consider the case where the transition region spans a finite number of nodes.

Again, a stationary solution should present a constant current throughout the entire system. Within the constant pressure drop regions $V_i = 1$, and the current is then J. A stationary solution requires the current in the intermediate region to be

$$V_i^2 \Gamma(\Delta P_i) = J, \tag{18}$$

where

$$V_i = 1 + \alpha(\Delta P_i - \Delta P_{i-1}). \tag{19}$$

We can rewrite Eq. (18) as

$$[1 + \alpha^2(\Delta P_i - \Delta P_{i-1})^2 + 2\alpha(\Delta P_i - \Delta P_{i-1})]\Gamma(\Delta P_i) = J. \tag{20}$$

Defining

$$\theta_i = \alpha(\Delta P_i - \Delta P_{i-1}), \tag{21}$$

Eq. (20) takes the form

$$\Gamma(\Delta P_i)\theta_i^2 + 2\Gamma(\Delta P_i)\theta_i + [\Gamma(\Delta P_i) - J] = 0, \tag{22}$$

which has the solution

$$\theta_i = -1 + \sqrt{J/\Gamma(\Delta P_i)}. \tag{23}$$

Note that we keep only the positive sign of the square root since $1 + \theta_i$ is the volume at node i. Using (21) we can write

$$\Delta P_i = \Delta P_{i-1} + \frac{1}{\alpha}[-1 + \sqrt{J/\Gamma(\Delta P_i)}]. \tag{24}$$

Let us now consider two cases, a piecewise pressure profile that connects a region of ΔP_a to a region of ΔP_c and the reverse (going from ΔP_c to ΔP_a). In the former case, the transition region is characterized by a $\Delta P_i = P_i - P_{i+1}$ that grows as i increases. If $\Gamma(\Delta P_i)$ has a local maximum at $\Delta P_{\max}$ followed by a local minimum at $\Delta P_{\min}$, as displayed in Fig. 2, Eq. (24) will have a solution for ΔP_i that grows from ΔP_a to ΔP_c only if

$$\alpha \leqslant \frac{-1 + \sqrt{J/\Gamma(\Delta P_{\min})}}{\Delta P_{\min} - \Delta P_a} \equiv \alpha_{c1} \tag{25}$$

(see the Supplemental Material [14] for the derivation). Similarly, in the case where a piecewise pressure profile connects a region of ΔP_c to a region of ΔP_a, $\Delta P_i = P_i - P_{i+1}$ must decrease in the transition region as i increases. Following similar arguments as before, (24) will have a solution if

$$\alpha \leqslant \frac{1 - \sqrt{J/\Gamma(\Delta P_{\max})}}{\Delta P_c - \Delta P_{\max}} \equiv \alpha_{c2}. \tag{26}$$

If α does not satisfy (25) or (26) these piecewise pressure profiles cannot be stationary solutions of the system.

In summary, when a constant pressure drop Π is applied to the network such that $\Pi/N = \Delta P_b$, with ΔP_b in the negative-slope region of $\Gamma(\Delta P)$, the homogeneous pressure profile ($\Delta P_i = \Delta P_b, \forall i$) is unstable. In addition, if $\alpha > \alpha_{c1}$ and $\alpha > \alpha_{c2}$, the piecewise pressure profiles discussed above are not stationary solutions. Performing numerical simulations in 1D networks (see the Supplemental Material [14]) we observe self-sustained oscillations outside these regions of stationary solutions. The next section provides a qualitative explanation of their behavior.

C. Traveling piecewise profiles

We have shown that the piecewise profiles shown in Figs. 2(b) and 2(c) can be stationary solutions of our model for α smaller than certain values. However, we can wonder if other piecewise profiles could move with some velocity across the system as traveling waves. An instance of this behavior is displayed in Fig. 3 where there is a pressure profile that travels from left to right while satisfying the boundary condition, a constant external pressure difference between the first and last node.

Consider again a piecewise profile where ΔP_i changes within an intermediate region from ΔP_a to ΔP_c. Since in that intermediate region $\Delta P_{i-1} < \Delta P_i$ we know $V_i > 1$, and this is a region of volume accumulation. If this volume accumulation were to be rigidly translated with speed c_a across the system, we can expect the pressure drop at any node within the system to change with time as $\Delta \dot{P}_i \sim -c_a(\Delta P_i - \Delta P_{i-1})$. Using Eqs. (5) and (19), one can define I, which is constant throughout the system,

$$I := \alpha \Delta \dot{P}_i + V_i^2 \Gamma(\Delta P_i) = \alpha \Delta \dot{P}_{i-1} + V_{i-1}^2 \Gamma(\Delta P_{i-1}). \tag{27}$$

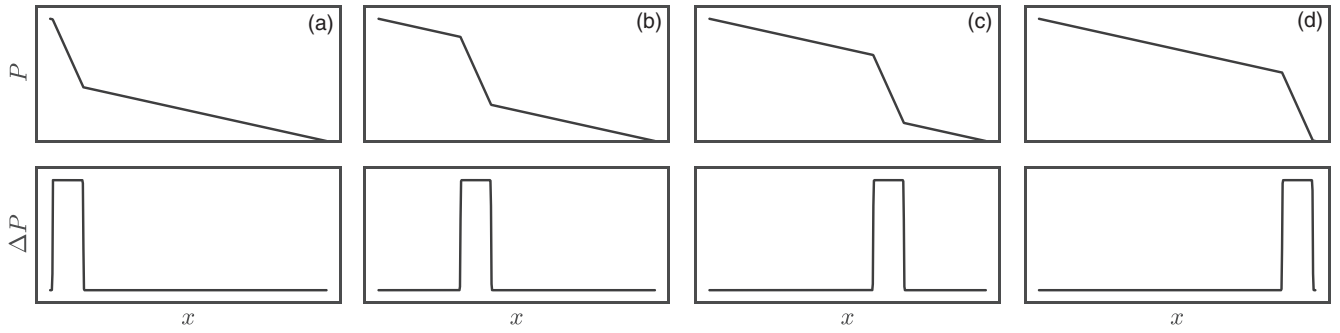

FIG. 3. A traveling wave through a system with constant pressure boundary conditions. The upper half of every panel depicts the pressure at every node of the system, whereas the bottom half shows the pressure drop at each node. These pressure profiles contain two transitions between ΔP_a and ΔP_c. The four panels correspond to different snapshots. The wave travels from left to right maintaining its shape [from panel (a) to (d)]. The wave can recycle once it reaches the end of the domain, satisfying the boundary conditions (a constant external pressure drop Π) at all times.

Using (27), the difference in pressure drop (ΔP) between the beginning and the end of the intermediate region can be rewritten as

$$\Delta P_c - \Delta P_a = \sum_i (\Delta P_i - \Delta P_{i-1}) = \sum_i \frac{-1}{c_a} \Delta \dot{P}_i$$
$$= \sum_i \frac{-1}{c_a \alpha} \left[I - V_i^2 \Gamma(\Delta P_i) \right] = \frac{1}{c_a \alpha} \left\{ \sum_i [\Gamma(\Delta P_i) - I] \right.$$
$$\left. + \sum_i [\alpha^2 (\Delta P_i - \Delta P_{i-1})^2 + 2\alpha (\Delta P_i - \Delta P_{i-1})] \Gamma(\Delta P_i) \right\}. \tag{28}$$

Solving for the velocity (c_a) we get

$$c_a = \frac{1}{(\Delta P_c - \Delta P_a)\alpha} \left\{ \sum_i [\Gamma(\Delta P_i) - I] \right.$$
$$\left. + \sum_i [\alpha^2 (\Delta P_i - \Delta P_{i-1})^2 + 2\alpha (\Delta P_i - \Delta P_{i-1})] \Gamma(\Delta P_i) \right\}. \tag{29}$$

One can follow similar steps for a profile where ΔP_i goes from ΔP_c to ΔP_a within the intermediate region (a volume depletion region) obtaining a similar expression c_d.

In general c_a and c_d can be different. The specific shape of the pressure profile (P_i and therefore ΔP_i) within these intermediate regions control the value of c_a and c_d. In fact, one accumulation and one depletion region can adapt their shapes, and thus their velocities, to travel together with the same speed. This creates a soliton-like traveling wave that always satisfies a constant pressure drop between the beginning and end of the system. This is schematically shown in Fig. 3. More detailed asymptotic analysis, as the ones performed for semiconductor dynamics lay outside the scope of this work. Asymptotic analysis concerning electronic dynamics in semiconductor heterostructures, which are described with a related model to our 1D case, can be found in [4].

IV. NUMERICAL RESULTS ON NETWORKS OF ARBITRARY TOPOLOGY

A. Boundary conditions and time integration of the model

The evolution of the system with time is determined by the evolution of the pressure field at every node P_i. Taking the derivative of Eq. (11) with respect to time and using Eq. (10) we get

$$\alpha \sum_k L_{ik} \dot{P}_k = -\sum_k I_{ik}. \tag{30}$$

To solve for $\dot{P}_i$ we need to consider the boundary conditions of the system of equations, i.e., we select n nodes from the system, set them as the contact points, and externally control their pressure. We assume that these nodes are reservoirs with a constant volume ($V_n = 1$). We augment the graph Laplacian by including the pressure boundary conditions as new rows and columns. For example, for the case where we consider two pressure contacts at nodes n_1 and n_2 we have

$$\hat{L}_{kl} = \begin{bmatrix} & & & & \vdots & \\ & & & & 0 & \vdots \\ & L_{ij} & & & 1 & 0 \\ & & & & 0 & 1 \\ & & & & \vdots & 0 \\ \dots & 0 & 1 & 0 & \dots & \vdots \\ & \dots & 0 & 1 & 0 & \dots \end{bmatrix}, \tag{31}$$

where the elements of the two new rows and columns are all zero except for $\hat{L}_{N+1,n_1} = \hat{L}_{N+2,n_2} = \hat{L}_{n_1,N+1} = \hat{L}_{n_2,N+2} = 1$. We also add corresponding elements to P_i and to the vector of currents,

$$\dot{\hat{P}}_k = \begin{bmatrix} \dot{P}_i \\ \lambda_1 \\ \lambda_2 \end{bmatrix}, \quad \hat{Q}_i = \begin{bmatrix} -\sum_k I_{ik} \\ \beta_1 \\ \beta_2 \end{bmatrix}, \tag{32}$$

to finally get

$$\dot{\hat{P}}_j = \frac{1}{\alpha} \sum_i \hat{L}^{-1}_{ji} \hat{Q}_i. \tag{33}$$

Note that in this formulation, from Eqs. (32) and (33), λ_i (with $i = 1, 2$) is related to the net currents going in (or out) of the system at node n_i, whereas β_i/α is the rate of change of the imposed pressure at the contact nodes. In general we will use as initial conditions $P_i = 0$ and $V_i = 1\ \forall i$. We carry out the time integration as follows. Starting from $P_{n_1} = 0$, we increase the pressure of n_1 at constant rate ($\beta_1 = \text{const}$, $\beta_2 = 0$) until it reaches the desired value Π. Then we set $\beta_1 = \beta_2 = 0$. Note that controlling β_i as a function of time enables to freely control the pressure at the contacts (n_1 and n_2). Integrating the system of equations contained in expression (33) with time we get the evolution of the pressure and volume in the system. Additionally, we obtain λ_0 and λ_1.

For an example of time integration see Fig. 4: Figs. 4(a) and 4(b), respectively, show a snapshot of the pressure and volume distribution in a planar disordered network, whereas Fig. 4(c) shows the total current at the contacts that is going in and out of the system with time. For this simulation we chose 10 pressure sources at random; in five of them (red nodes) the pressure is 0 during the whole simulation. For the other five contacts (blue nodes) the pressure is ramped up at a fixed rate to a constant value of 150 and kept constant afterwards. After a brief transient, the system exhibits stable disordered volume waves that travel through the system all while satisfying time-independent pressure boundary conditions. Figure 4(c) shows oscillations in the total current that is going in and out of the system.

B. Results

The aim of this section is to present and explain different instances of the rich behavior that this model can display in one and two dimensions. We begin by an exploration of the behavior of the 1D network, where we can directly compare our analytical predictions in Sec. III with the results of the simulation. For the 1D system we present a phase diagram that summarizes the different types of behavior the system can exhibit. We also demonstrate that the network can behave as an excitable medium. We then move to two-dimensional (2D) networks, where we first demonstrate the highly complex patterns of dynamics that can be present when more than two contact points are present, a behavior that is intrinsically absent from one dimension. Last, we demonstrate that in two dimensions the system exhibits qualitative similarities in behavior with excitable systems such as the one in [15].

1. Phase diagram and robustness of the dynamical behavior

In Fig. 5 we present a phase diagram for a 1D network of $N = 100$ nodes. For each value of α and Π we perform an independent simulation. Π is the pressure difference between the two extremes, the contact points. The initial conditions are $V_i = 1$ and $P_i = 0$, $\forall i$. For $t > 0$ we ramp up the pressure at one contact point until it reaches Π and keep it fixed afterwards. The pressure at the other contact point is fixed at 0. The protocol of gradual ramping up of the pressure at the contact point was chosen because of its connection to experiments (the system starts disconnected from the pressure source, so that all internal points are initially at zero pressure). The arbitrary choice of initial conditions generally only affects the transient and not the eventual dynamic or stationary steady state.

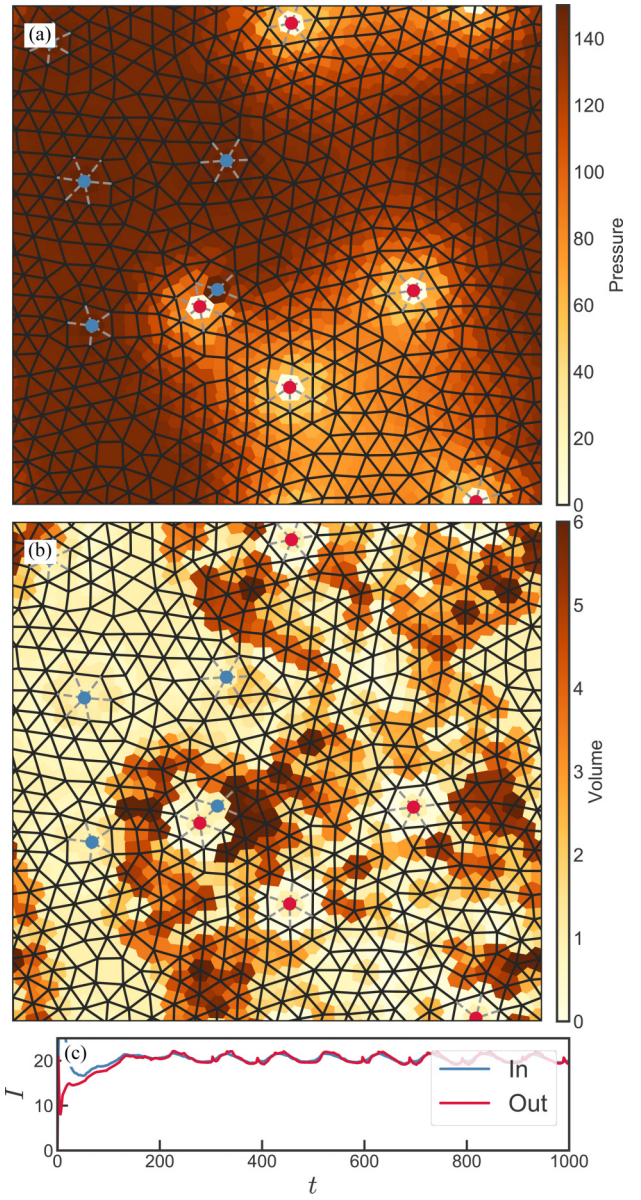

FIG. 4. Volume waves on a disordered planar network. The two upper panels show the pressure (a) and volume (b) distribution at dimensionless time 1000. The value of P_i and V_i is represented by the color surrounding each node. The network has 512 nodes and an average degree of ~5.5. We have placed 10 contacts at random (blue and red dots). The pressure increases at constant rate, $\beta_1 = 5$, at the blue contacts until they reach a value of pressure $P = 150$ and remains constant afterwards. The pressure at the red contacts is always 0. All edges in the network follow Γ_{NL} with $\epsilon = 0.001$ (continuous lines), except for the edges connected to one of the contacts that follow Γ_L with $h = 1/5$ (dashed lines). We used $\alpha = 0.32$. Panel (c) shows the evolution of the current that is going in (blue) and out (red) of the system with respect to time. Note that the system is undergoing self-sustained oscillations where volume waves travel across the system (with periodic boundary conditions) until they reach another contact.

Figure 5 exhibits a region of oscillatory behavior. The phase diagram also contains the analytical predictions that

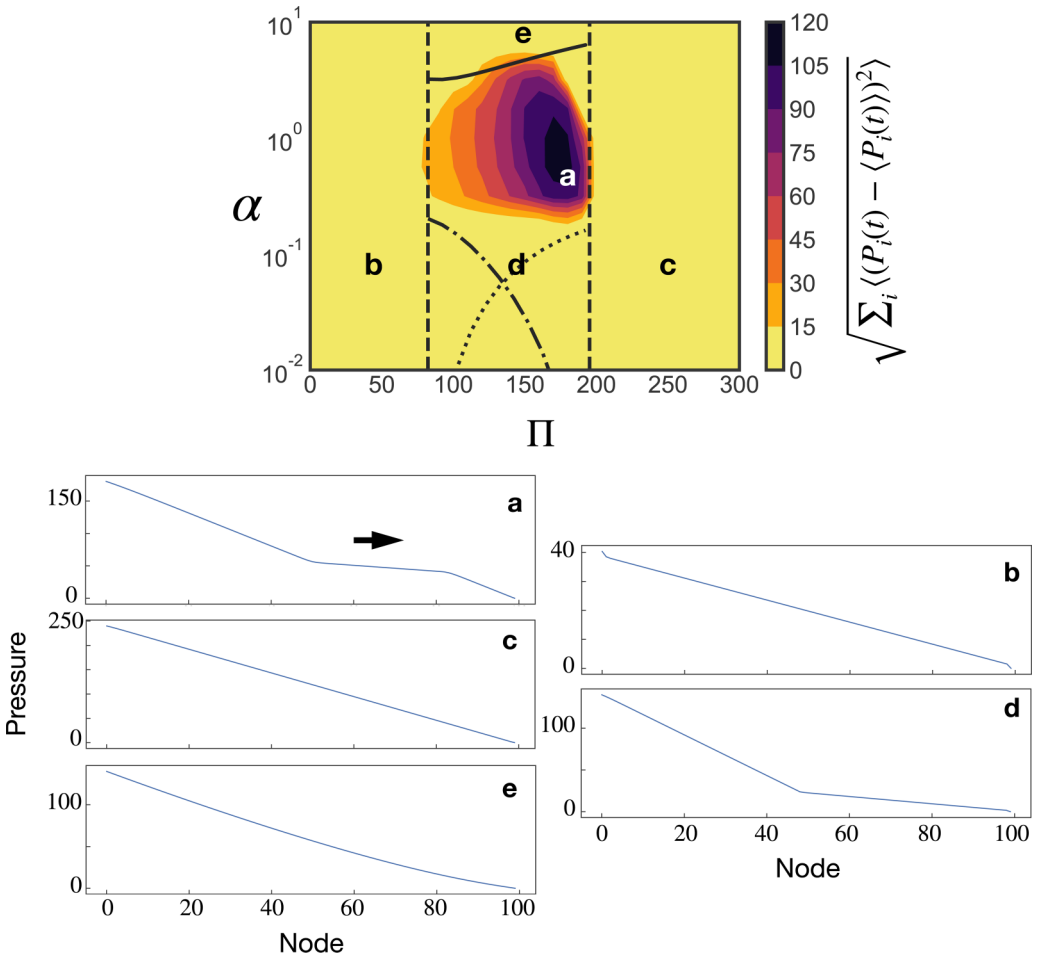

FIG. 5. Phase diagram for a 1D network of 100 nodes, $\epsilon = 0.15$ and $h = 1/5$. Color map indicates the amplitude of the oscillations. Vertical dashed lines correspond to $100\Delta P_{\min}$ and $100\Delta P_{\max}$. Dotted and dashed-dotted lines correspond to expressions (25) and (26), respectively. The continuous line corresponds to expression (36). Note how the oscillations occur in the region delimited by the analytical bounds. Panels below the phase diagram show the pressure profile throughout the network at the points marked with letters (a)–(e). (a) A snapshot of the time-dependent pressure profile that corresponds to the region of largest oscillations. Note that it has the structure proposed in Fig. 3; (b) and (c) two linear stationary pressure profiles, as the theory predicts; (d) piecewise stationary profile, as described in Sec. III B; (e) stationary pressure profile with curvature ($V_i < 1$), as our analytical results predict for large values of α.

constrains the region where we expect to see oscillations, in good agreement with the numerical results. The two vertical dashed lines limit the region at which the homogeneous stationary solution is unstable; see Sec. III A. For larger or smaller pressure differences (Π) we expect to see linear pressure drops, as Figs. 5(b) and 5(c) confirm. Below the dotted and dashed-dotted lines piecewise stationary profiles are stable; see Sec. III B. This is in good agreement with Fig. 5(d). Figure 5(a) shows a snapshot of the time evolution of the pressure profile for a point in the phase diagram where the system displays self-sustained oscillations. The pressure distribution in this case is formed by three linear pieces, as described in Sec. III C (see also Fig. 3).

Finally, we would like to understand why the oscillations disappear for large α. As shown in Figs. 3 and 5(a), self-oscillations occur for piecewise solutions that contain two transition regions, one where $V_i > 1$ and another where $V_i < 1$. For a total pressure decay $\Pi = N\Delta P_b$ (where $\Delta P_{\min} < \Delta P_b < \Delta P_{\max}$), we know that the pressure drop inside the accumulation region ($V_i > 1$) goes from ΔP_a to ΔP_c, whereas the pressure drop inside the depletion region ($V_i < 1$) goes from ΔP_c to ΔP_a, see Fig. 2. Moreover, we know that volume always has to be positive. Using (12) and $V_i > 0$ we get

$$1 + \alpha(\Delta P_i - \Delta P_{i-1}) > 0. \tag{34}$$

When the system displays oscillations, the transition regions should occupy a small portion of the network, see Sec. III C and Fig. 5(a). A traveling wave has two narrow depletion or accumulation regions separated by a linear pressure drop domain. Such a traveling wave cannot be maintained if the depletion or accumulation regions are comparable to the size of the system. If we suppose that the depletion region occupies approximately 10% of the entire system, or $N/10$ nodes, we can approximate (34) by

$$1 + \alpha \frac{\Delta P_a - \Delta P_c}{N/10} > 0, \tag{35}$$

which translates to

$$\alpha < \frac{10}{\Delta P_c - \Delta P_a}, \tag{36}$$

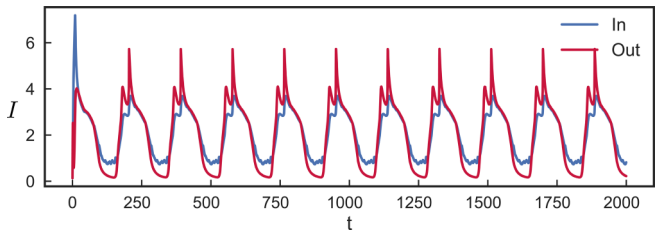

FIG. 6. Self-sustained oscillations in a regular cubic network of dimensions $7 \times 7 \times 7$ with two contacts connected to two opposite corners. The plot shows the current going in and out of the system during a simulation displaying self-sustained oscillations. Parameter values are $\alpha = 0.32$, $\Pi = 150$, $\epsilon = 0.001$, $h = 1/5$, $\beta_1 = 5$ ($\beta_1 = 0$ when P_1 reaches the desired value) and $\beta_2 = 0$.

for $N = 100$. We include expression (36) in Fig. 5 with a continuous line, below which we expect to see oscillations. According to this, for α above the continuous line the depletion region ($V_i < 1$) has to occupy a larger fraction of the nodes of the network to be able to respect the $V_i > 0$ condition. This does not allow the traveling wave to develop. This is in good agreement with Fig. 5(e), which shows a depletion region that occupies almost the complete network (note the subtle curvature of the pressure profile what implies $V_i < 1$).

The maximum fraction of the traveling wave occupied by the accumulation and depletion regions was estimated at 10%. However, note that a factor of 2 increase or decrease in that fraction would still provide qualitatively good agreement with the simulation, as the region of the phase diagram that exhibits oscillations spans almost two decades.

Additionally, our work indicates that the emergence of complex dynamics in this model is a robust effect that persists after modifying different properties of the system. To show this, we present in the Supplemental Material [14] phase diagrams for 1D networks, with different shapes of Γ_{NL} and Γ_L and different distributions of linear edges. Self-sustained complex dynamics are found for a broad range of α and Π values. Complex dynamics are also present in nonplanar networks. To illustrate this, we include here a simulation carried out using a cubic lattice, also displaying self-sustained oscillations; see Fig. 6.

2. *Excitability*

In this work we have focused more extensively in the oscillatory regime of the system where time-independent pressure boundary conditions result in time-dependent behavior. However, one of the distinctive features of this model is its capacity to get exited by external perturbations. Excitable media, according to classical definitions (e.g., [8]), show large excursions in phase space after being driven away from an equilibrium point, for a certain range of their parameters. In this subsection we show how our system responds to a pressure perturbation while within the excitable regime of the system.

In Fig. 7 we show a simulation in a rectangular network with 5×100 nodes. Figures 7(a)–7(g) present snapshots of the volume distribution in the system at different times, whereas Fig. 7(h) shows the current that is going in and out of the system, and Fig. 7(i) presents the pressure at the contact

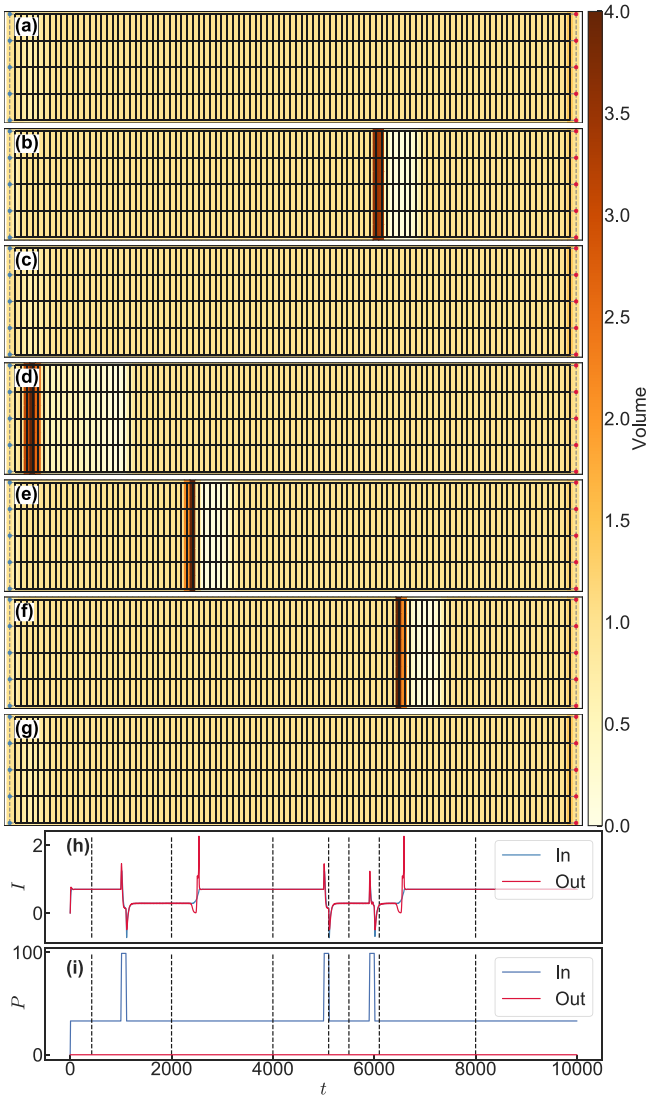

FIG. 7. Excitability of a network with 500 nodes arranged in a rectangular grid, with five rows and 100 columns. The pressure of the red nodes in the right column ("Out" nodes) is maintained constant at 0, whereas the pressure of the nodes in the left column ("In" nodes) follows the protocol displayed in blue in panel (i). Panels (a)–(g) display the volume at each node of the network for the different times marked in (h) and (i) with vertical dashed lines. Continuous lines in (a)–(g) stand for edges following Γ_{NL}, whereas dashed gray lines stand for Γ_L (present only around the contacts). $\epsilon = 0.001$, $h = 1/5$, and $\alpha = 1$. Panel (h) displays the current that goes in and out of the system as a function of time. For this configuration the system is stable around a state with a homogeneous volume distribution (panels a, c, and g). A short perturbation in the pressure (i) can trigger a pulse that propagates along the complete network. A second pulse cannot be excited while one is still traveling through the network (f).

points versus time. In the simulation, we rapidly increase the pressure at the blue nodes and keep it constant at $P = 40$, a stable point of the system with an homogeneous volume distribution [Fig. 7(a)]. We then perturb the system with a brief increase of the pressure on the boundary. This triggers a pulse that travels through the system [a large excursion in phase space; see Fig. 7(b)]. After the pulse arrives to the

other end of the network (the low-pressure contact points), the system is in its stable point again [Fig. 7(c)]. We then trigger another pulse [Fig. 7(d)], and while it is traveling through the system we introduce a third perturbation. However, the presence of the previous pulse prevents the creation of a new one and gives rise to an effective "refractory" time for the traveling excitation [see Fig. 7(f)]. Finally, with no more perturbations the system returns to the equilibrium behavior again, after the last pulse has exited the low-pressure contact points [Fig. 7(g)].

3. The spatial footprints of traveling waves

When waves travel through networks of nonlinear resistors, they follow complex spatial-temporal patterns that depend on the network topology and position and number of contact points, something not present in the 1D analysis. In Fig. 8 we show three different sets of pressure boundary conditions for a disordered planar network: two, six, and ten contacts (one case per column). Each configuration produces a different oscillatory pattern, where the volume stored in some nodes oscillates with a large amplitude, whereas the volume stored at other nodes is almost stationary. We display three snapshots for every configuration, panels (a)–(c) for the case with two contacts, panels (e)–(g) with six contacts, and panels (i)–(k) with 10 contacts. The bottom row (panels (d), (h) and (l)) displays the standard deviation of the time series of the accumulated volume at each node. In simple cases with a small number of contact points, these static profiles have spatial distributions that resemble the temporal-spatial patterns shown in the snapshots. In particular, conservation of mass imposes that pulses that change their shape increase their amplitude as they concentrate in smaller regions. This causes the standard deviations [panels (d), (h), and (l)] to highlight regions close to the contacts, with shapes that resemble the pulse fronts. For the case with two contacts (a)–(c), note that the volume wave front near the low-pressure contact point is radially symmetric, but near the high-pressure contact point the profile is dendritic. As the number of contact points increases then the oscillatory patterns become more complex. The standard deviation of the time-dependent volume stored at each node is highly variable. The magnitude of the fluctuations does not follow the simple patterns of the two-contact case. Instead, we find regions close to the contact points that oscillate strongly and regions close to them that are stationary. We hypothesize that these complex spatiotemporal patterns are partially due to constructive and destructive interference of the traveling waves, but the detailed study of the patterns is not in the scope of this work.

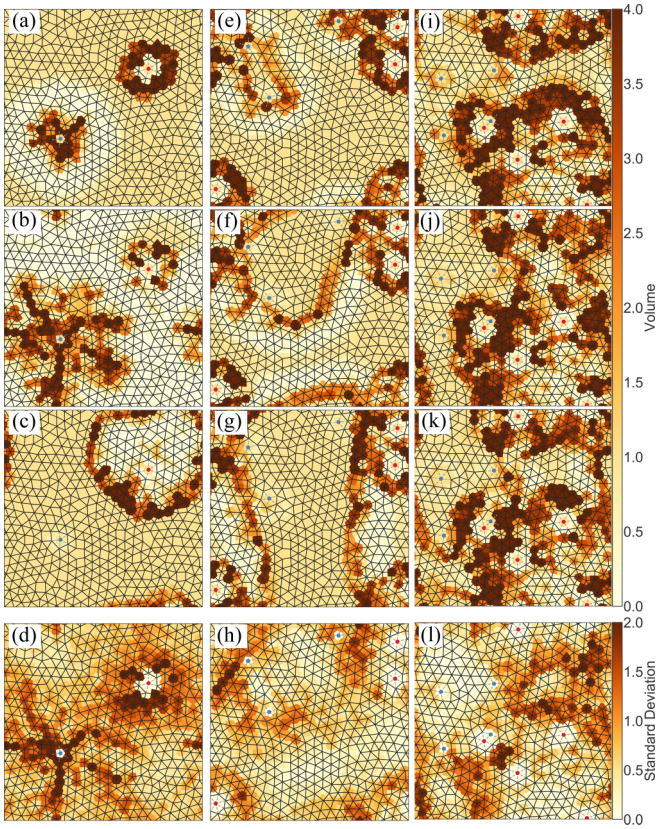

FIG. 8. Self-sustained oscillations for different sets of contact points. Rows 1 to 3 (panels (a), (b), (c), (e), (f), (g), (i), (j), and (k)) correspond to snapshots whereas the bottom row (panels (d), (h), and (l)) corresponds to the standard deviation of the volume at each node (it is calculated from the volume time series at every node). The color coding stands for volume accumulated at each node. We use a disordered planar network with 512 nodes, average connectivity ~5.5, and periodic spatial boundary conditions. Continuous lines stand for edges following $\Gamma_{\rm NL}$, whereas dashed gray lines stand for Γ_L (here present only around the contacts). We used $\epsilon = 0.001$, $h = 1/5$, $\alpha = 0.32$, and $\Pi = 150$ for all simulations. Pressure is maintained constant at 150 at the blue nodes, and 0 at red nodes. Left column (panels (a), (b), and (c)) presents waves traveling from one high-pressure contact to a low-pressure one. Central column (panels (e), (f), and (g)) shows snapshots of traveling waves for six randomly distributed contacts points (three corresponding to high pressure and three for low pressure). Right column (panels (i), (j), and (k)) presents an analogous case but with 10 contacts points (five corresponding to high pressure and five for low pressure). The bottom row (panels (d), (h), and (l)) shows the profiles obtained after computing the standard deviation of the volume time series at each node. This is done after the initial transient has passed and the system displays stable oscillations.

4. Regions of linear conductance

As we have discussed in other sections, it is the combination of the nonlinear conductance and the coupling between volume and pressure that gives rise to complex dynamics. In this section, motivated by [15], we study how traveling waves interact with a region of linear edges. To achieve this we take a disordered planar network without periodic spatial boundary conditions (see Fig. 9). We impose a constant high pressure to the contacts on the left boundary of the system and zero pressure to the contacts on the right. After a short transient, approximately flat fronts move from left to right; see snapshots in Figs. 9(a)–9(c). Now we modify the conductance of the edges in a circular region in the middle of the network, making them linear [following $\Gamma_L(\Delta P)$]. When the fronts arrive to the linear region, they "leap frog" ahead and continue their propagation at the other side; see Figs. 9(d)–9(f). Finally, we do the same with a larger region in panels (g)–(i). These results are consistent with linear regions being areas of very

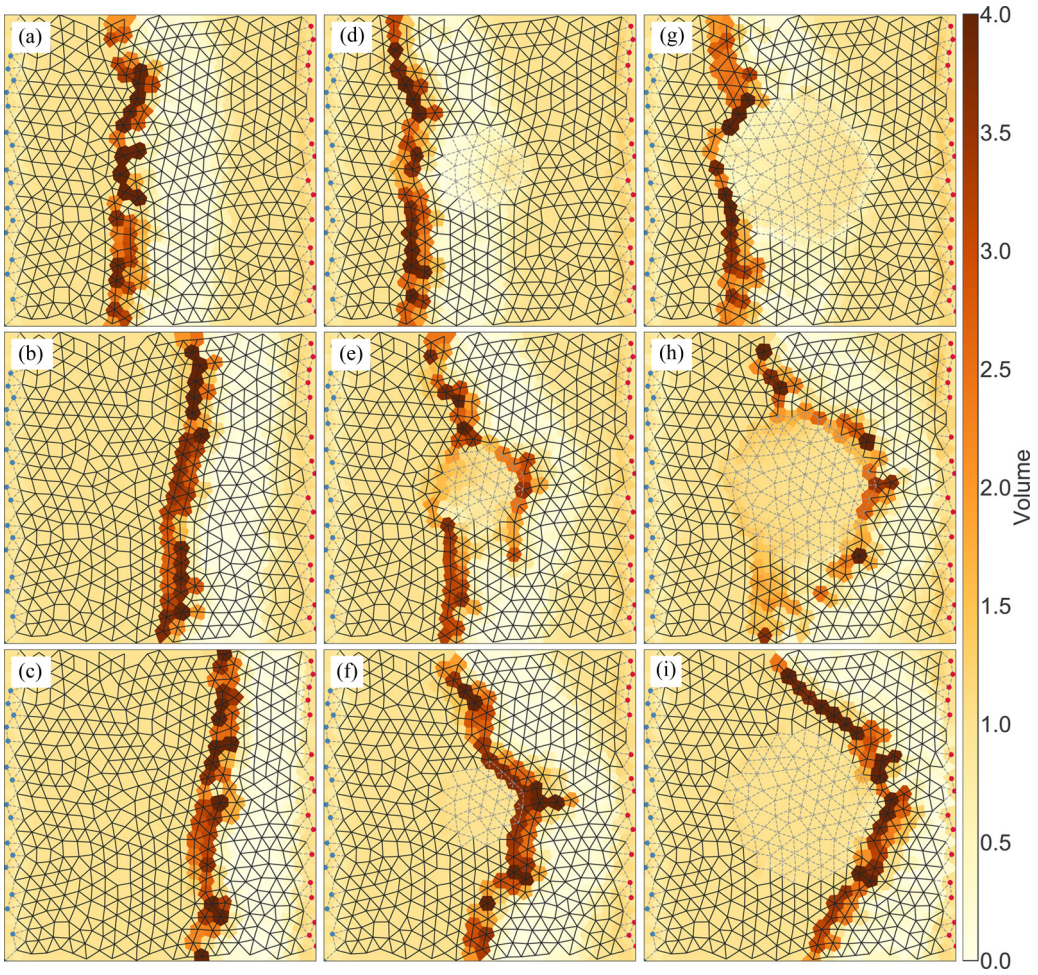

FIG. 9. Snapshots of planar waves traveling through a region of linear conductance. Color patches around each node stand for volume accumulated at that node. We use a disordered planar network with 512 nodes and average connectivity ~5.5, without spatial periodic boundary conditions. Continuous lines stand for edges following Γ_{NL} whereas dashed gray lines stand for Γ_L. We used $\epsilon = 0.001$, $h = 1/5$, $\alpha = 0.32$, and $\Pi = 35$ for all the simulations. Pressure is maintained constant at 35 at the left blue nodes, and 0 at the right red nodes. (a)–(c) Snapshots of planar waves traveling from left to right. (d)–(f) Illustration of how the planar wave gets distorted when it reaches a central region of linear edges (35 linear edges). (g)–(i) An analogous case but with 98 linear edges in the central region. The waves "leap frog" the linear edges. This leads to an increase of the oscillation frequency, as the waves can traverse and exit the system faster.

fast pulse propagation. The observed behavior is reminiscent of that shown in Figs. 3(a)– 3(c) of Ref. [15], further strengthening the connection of the phenomenology of the model with standard excitable systems.

V. DISCUSSION

The work contained in this paper presents a model to study dynamics on complex networks. We use general phenomenological expressions that can be applied to a broad variety of problems. Indeed, these expressions can be modified and adapted to make them better approximate the governing equations of other physical or biological systems. We therefore expect the framework presented in this work to open new research avenues in the study of dynamics in nonlinear flow networks of arbitrary topology. One such potential example is the spontaneous fluctuations of blood volume in the brain vasculature [16]. It has been proposed that spontaneous fluctuations (in resting state) may be due to a nonneural origin [17], in contrast to typical brain hemodynamics, which is driven by the activity of neurons. Understanding and modeling these phenomena in brain vasculature is of critical importance, since functional magnetic resonance imaging (fMRI) relies on the tight correlation of neural activity with blood volume and oxygenation. We have included in Appendix B a brief discussion of the physical arguments that may connect our model to brain hemodynamics. Brain blood flow dynamics is not the only biological system where spontaneous oscillations arise. Another system that involves intrinsic peristaltic-like contractions (which are also poorly understood) is the lymphatic system [18].

In summary, this work shows how a network of nonlinear resistors can display emergent spontaneous dynamics for very different topologies and boundary conditions. The analytical results of Sec. II help to understand the basic mechanisms behind the emergence of this complex behavior. We have shown how the negative-slope region makes the "trivial" homogeneous solution unstable in some cases, and how the system

can support traveling waves. More detailed analysis of similar models in one dimension can be found in the semiconductor heterostructure literature (see, e.g., [3,4]).

In Sec. IV A we discussed how to numerically integrate the system of equations for the case of a network of arbitrary topology. To do so we showed how to include the pressure boundary conditions as a redefinition of the graph Laplacian. This enabled us to integrate the system numerically in a straightforward way, obtaining the time-dependent pressure and volume at each node. This is a completely different approach from the one used to time integrate the equations of the models studying semiconductor superlattices [3]. Since those cases were 1D the integration could be performed using one Lagrange multiplier. Our approach is more general and suitable for networks of arbitrary topology. In addition, our model opens the possibility of exploring other types of complex dynamics in flow networks, as it provides a general framework to explore systems with different expressions for edge conductance or for the volume-pressure coupling.

We have extensively discussed how the combination of nonlinear edges and the coupling between pressure and volume can give rise to emergent spontaneous fluctuations under time-independent pressure boundary conditions. These systems present a broad array of interesting phenomena that will encourage further research, like the complex spatial patterns of volume fluctuations or the traveling wave behavior in inhomogeneous media composed of regions of linear edges. Moreover, in Sec. IV B 2 we discussed how this model presents some properties which are typical of an excitable medium [8] while still in the realm of distribution network theory. In this way we believe this model is an example of a new class of excitable systems, different from other models of excitable networks that explicitly use excitable elements in their nodes [9,10]. Instead, our excitable flow network is composed of edges that present a nonlinear conductance and nodes that can store volume. The excitable nature of the system emerges as a product of the global coupling between currents, volumes, and pressures.

ACKNOWLEDGMENTS

This research was supported by the National Science Foundation via Award No. DMR1506625 (M.R.-G.), and the Simons Foundation via Award No. 454945 (M.R.-G.). E.K. acknowledges partial support by NSF Award PHY-1554887, the University of Pennsylvania Materials Research Science and Engineering Center (MRSEC) through Award DMR-1720530, the University of Pennsylvania CEMB through Award CMMI-1548571, and the Simons Foundation through Award 568888.

APPENDIX A: COUPLING BETWEEN VOLUME ACCUMULATION AND PRESSURE IN FLEXIBLE TUBES

We consider a network of flexible tubes embedded in an elastic (almost incompressible) medium. The deformation of the tube wall and the surrounding medium controls the pressure response to a local volume accumulation. This relation is included in our model through the phenomenological relation (4). This equation is nonlocal, which means that an accumulation of volume causes a increase of pressure not only in the region of accumulation but also in neighboring sites. In particular, a local volume accumulation in relation (4) produces a pressure field that decays with distance from the region of accumulation.

Here we test whether a local volume accumulation inside a hollow vessel embedded in an elastic medium could produce a decaying pressure field. In particular, we solve the equilibrium equations of classical linear elasticity [19],

$$\frac{E}{2(1+\sigma)}\frac{\partial^2 u_i}{\partial x_k^2} + \frac{E}{2(1+\sigma)(1-2\sigma)}\frac{\partial^2 u_l}{\partial x_i \partial x_l} = 0, \qquad \text{(A1)}$$

where u_i are the components of the displacement vector field, E is the Young's modulus, σ is the Poisson's ratio, and x_i are the spatial variables; summation over repeated indices is implicit.

For simplicity, we use a rectangular domain as a 2D version of our problem, and we clamp all its boundaries except for the region $\partial\Omega_{\text{free}} \equiv (y = 0,\ x_i < x < x_f)$; see Fig. 10. The lower boundary ($y = 0$) of the elastic medium is meant to represent the interface between the tube (that carries the fluid) and the medium that embeds it. We impose a vertical pressure on the free "surface" ($\partial\Omega_{\text{free}}$) with a bump shape, $P_{\text{ext}} = 30e^{(-1/\{0.25-[(x-x_i)/(x_f-x_i)-0.5]^2\})}$, displayed in Fig. 10(f). As the rest of the lower boundary is clamped, we can measure the pressure that the medium exerts on the nondeformed region of the tube. In the presence of fluid in the tube, this pressure field would promote flows that would give rise to new deformations, a phenomenology that is described in the rest of this work.

Finally, the pressure field exerted by the medium on its lower boundary [$\sigma_{yy}(y = 0)$] is displayed in Fig. 10(a). To illustrate this effect, we use four different values of the Poisson's ratio, although only values close to 0.5 are probably relevant in most experimental cases. All lines collapse in $\partial\Omega_{\text{free}}$, as expected since they need to cancel the externally applied pressure. Outside this region ($x < x_i,\ x_f < x$), there is a pressure field whose magnitude decays with the distance to the volume accumulation, and the direction depends on the sign of σ. For positive Poisson ratios (the most relevant situation) the direction of the pressure response is against the tube wall, in qualitative agreement with expression (4). For visualization, we also plot the deformations undergone by each material using a simplified mesh [see Figs. 10(b)–10(e)].

APPENDIX B: POSSIBLE SOURCES OF NONLINEARITIES IN BIOLOGICAL SYSTEMS

The model contained in this work describes the emergence of complex dynamics in flow networks, allowing for local volume accumulation within the system and nonlinear conductances for the edges. In this Appendix we describe various phenomena in the mammalian brain vasculature that could potentially produce complex nonlinear behavior for the conductance of the vessels, reminiscent of the nonlinearities present in $\Gamma(\Delta P)$.

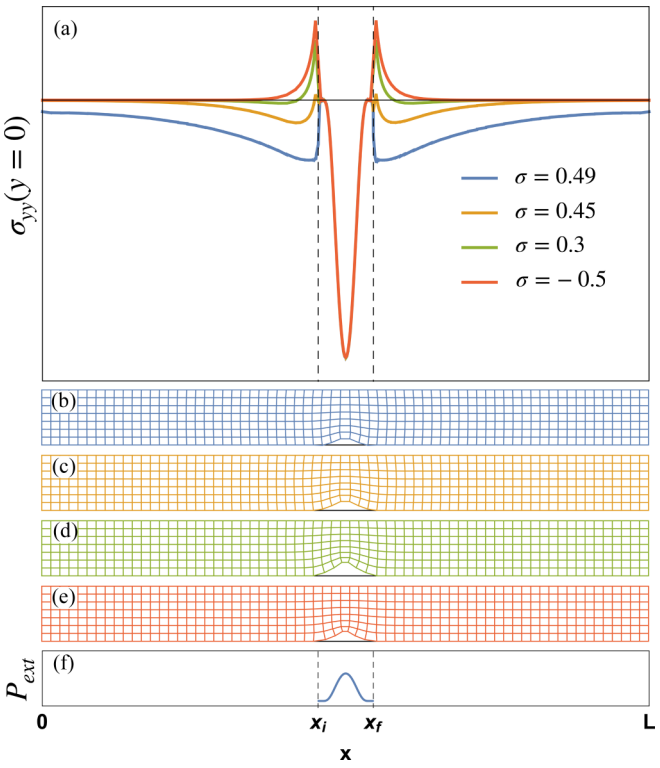

FIG. 10. Idealized deformation of the medium surrounding a volume accumulation inside a flexible tube and associated stresses. We consider rectangular domains with different Poisson ratios. The boundaries are clamped (displacements, u_1 and u_2, are set to zero), except for a free "surface" ($y = 0$ and $x_i < x < x_f$) where we impose an external pressure (f). In panel (a) we measure the pressure that the medium imposes on the vessel, $\sigma_{yy}(y = 0)$. All lines collapse in the free surface region, canceling the imposed external pressure. Outside this region different Poisson ratios produce different pressure profiles that decay away from the free surface region. For large Poisson ratios the deformation of the surrounding medium produces a pressure field of negative sign (against the tube), qualitatively analogous to the pressure-volume relation that we use in our model. The displacements present in each of the cases are displayed in panels (b)–(e), where the meshes have been simplified for easier visualization. Dashed lines in (a) and (f) mark the region where the external pressure is applied.

Different vessels present in the mammalian brain vasculature display a broad and complex response to changes in pressure or flow conditions. This response can be active, when the vessel modifies its muscle tone, or passive, controlled only by the fluid-mechanical interaction between the blood and the vessel. A detailed account of all effects lays outside the scope of this work. However here we present a short review for the interested reader.

Active nature of vessels. Since the seminal work of Bayliss in 1902 [20], it is known that vessels can present a myogenic response, as they constrict in response to an increment of internal pressure. Flow has also been experimentally found to cause dilation and contraction of vessels [21]. This response depends on different factors, such as the internal pressure [22] and the ability of endothelial cells to sense blood flow [23]. Experimental work [22,24] is consistent with a nonmonotonic $\Gamma(\Delta P)$ function. The dilation of the vessel in response to sheer stress is nonmonotonic for low and intermediate myogenic tone. As sheer stress increases, the vessel dilates until it reaches a maximum radius and then reduces the radius for larger sheer stress. That causes a nonmonotonic relation between flow and pressure difference. In addition, some experimental work has shown an oscillatory myogenic response to a constant internal pressure [25]. We do not consider this effect in our model although it could be included as edges presenting a time-dependent $\Gamma(\Delta P)$.

Passive response. It has been theoretically proposed [26] that a viscous flow through a flexible tube can become unstable. When the pressure difference between the ends of the tube reaches a critical value, any small perturbation in the flow will exponentially grow producing a deformation of the flexible tube and making the fluid flow depart from the laminar behavior. This sudden change increases the energy dissipated in the system and results in a consequent drop of the total flow. This type of instability has been experimentally measured in [27,28], where the authors observed a sudden increase of the effective viscosity of the fluid due to the development of the instability. This would be consistent with the nonmonotonic flow-pressure relation used in this work. The critical velocities for which the linear stability analysis of [26] gives the first unstable mode is of the order of cm/s for a vessel with a diameter of 100 μm and of the order of mm/s for a 5 μm capillary, in good agreement with typical blood velocities [29]. Nonetheless, this passive response still needs to be measured experimentally in real blood vessels. In addition to this, blood rheology may also play an important role since blood is a complex fluid whose constituent agents are deformable and very often of the order of the vessel radius [29,30].

[1] G. Kirchhoff, Ann. Phys. **148**, 497 (1847).
[2] C. Murray, Proc. Natl. Acad. Sci. USA **12**, 207 (1926).
[3] L. L. Bonilla and H. T. Grahn, Rep. Prog. Phys. **68**, 577 (2005).
[4] L. L. Bonilla and S. W. Teitsworth, *Nonlinear Wave Methods for Charge Transport* (Wiley, Leipzig, 2010).
[5] M. Ruiz-Garcia, J. Essen, M. Carretero, L. L. Bonilla, and B. Birnir, Phys. Rev. B **95**, 085204 (2017).
[6] J. Essen, M. Ruiz-Garcia, I. Jenkins, M. Carretero, L. L. Bonilla, and B. Birnir, Chaos **28**, 043107 (2018).
[7] L. L. Bonilla and F. J. Higuera, SIAM J. Appl. Math. **55**, 1625 (1995).
[8] M. C. Cross and P. C. Hohenberg, Rev. Mod. Phys. **65**, 851 (1993).
[9] O. Kinouchi and M. Copelli, Nat. Phys. **2**, 348 (2006).
[10] A. Roxin, H. Riecke, and S. A. Solla, Phys. Rev. Lett. **92**, 198101 (2004).
[11] J. Alvarado, J. Comtet, E. de Langre, and A. Hosoi, Nat. Phys. **13**, 1014 (2017).

[12] A. H. Christensen and K. H. Jensen, Phys. Rev. Fluids **5**, 044101 (2020).
[13] J.-F. Louf, J. Knoblauch, and K. H. Jensen, Phys. Rev. Lett. **125**, 098101 (2020).
[14] See Supplemental Material at http://link.aps.org/supplemental/10.1103/PhysRevE.103.062301 for numerical and analytical results complementing the theory described in this paper. There are also two videos that display traveling waves and excitable behavior in nonlinear flow networks.
[15] V. Zykov, A. Krekhov, and E. Bodenschatz, Proc. Natl. Acad. Sci. USA **114**, 1281 (2017).
[16] M. D. Fox and M. E. Raichle, Nat. Rev. Neurosci. **8**, 700 (2007).
[17] A. T. Winder, C. Echagarruga, Q. Zhang, and P. J. Drew, Nat. Neurosci. **20**, 1761 (2017).
[18] K. Margaris and R. A. Black, J. R. Soc., Interface **9**, 601 (2012).
[19] L. D. Landau and E. M. Lifshitz, *Theory of Elasticity* (Pergamon Press, Oxford, New York, 1986).
[20] M. W. Bayliss, J. Physiol. **28**, 220 (1902).
[21] J. A. Bevan and I. Laher, FASEB J. **5**, 2267 (1991).
[22] N. Thorin-Trescases and J. A. Bevan, Stroke **29**, 1194 (1998).
[23] K. Yamamoto, T. Sokabe, T. Matsumoto, K. Yoshimura, M. Shibata, N. Ohura, T. Fukuda, T. Sato, K. Sekine, S. Kato *et al.*, Nat. Med. **12**, 133 (2006).
[24] A. C. Ngai and H. R. Winn, Circ. Res. **77**, 832 (1995).
[25] G. Osol and W. Halpern, Am. J. Physiol. **254**, H28 (1988).
[26] V. Kumaran, J. Fluid Mech. **294**, 259 (1995).
[27] V. Kumaran and R. Muralikrishnan, Phys. Rev. Lett. **84**, 3310 (2000).
[28] R. Neelamegam, D. Giribabu, and V. Shankar, Phys. Rev. E **90**, 043004 (2014).
[29] T. W. Secomb, Annu. Rev. Fluid Mech. **49**, 443 (2017).
[30] Y. C. Fung, *Biomechanics* (Springer Science & Business Media, New York, 2013).